Photothermal Conversion of Solar Infrared Radiation by Plasmonic Nanoantennas for Photovoltaic-Thermoelectric Hybrid Devices

Sébastien Hanauer, Inès Massiot, Adnen Mlayah, Franck Carcenac, Jean-Baptiste Doucet, Sélyan Beldjoudi, Ihar Faniayeu, Alexandre Dmitriev

Photothermal conversion of solar infrared radiation by plasmonic nanoantennas for photovoltaic-thermoelectric hybrid devices

Sébastien Hanauer,[†] Inès Massiot,[*,†] Adnen Mlayah,[†] Franck Carcenac,[†] Jean-Baptiste Doucet,[†] Sélyan Beldjoudi,[†] Ihar Faniayeu,[‡] and Alexandre Dmitriev[‡]

[†]*LAAS-CNRS, Université de Toulouse, CNRS, 7 avenue du Colonel Roche, 31400 Toulouse, France*

[‡]*Department of Physics, University of Gothenburg, 41296 Gothenburg, Sweden*

E-mail: ines.massiot@laas.fr

Abstract

Photovoltaics have become one of the low-cost options for electricity generation. However, the lack of absorption of the near-infrared and infrared solar spectrum intrinsically limits its efficiency. Here, we present an approach for photothermal conversion of solar infrared radiation in photovoltaic-thermoelectric systems using plasmonic nanoantennas. Through numerical calculations-driven shape engineering we identified Ni diabolo nanoantennas as efficient solar infrared spectrum harvesters. Nanofabrication with electron-beam lithography further revealed its impact on nanoantennas optical properties at single-nanoantenna level. In the large-scale low-cost approach, however, photothermal surfaces of nanocone plasmonic antennas, made with a simple and robust fabrication process, still deliver a significant 6.1°C temperature increase under solar

infrared illumination. The reported results pave the way towards the development of hybrid photovoltaic-thermoelectric systems with an optimal utilization of the solar spectrum.

Keywords

hybrid energy harvesting, thermoelectricity, photovoltaics, photothermal conversion, interface layer, thermoplasmonics.

One of the key issues at stake in a society full of energy-consuming devices is to design and build self-sufficient energy systems. A winning strategy could be to make the most out of ambient energy, including the most abundant energy source on Earth: solar. Solar photovoltaics is one of the lowest-cost options for electricity generation.[1] However, no matter the photovoltaic material, the conversion efficiency of a solar cell is fundamentally limited by intrinsic losses.[2] As illustrated in Figure 1A, the efficiency of a single-junction solar cell (with an energy bandgap E_g) suffers from two main channels of losses, the thermalization of photons with an excess energy ($E > E_g$) and the lack of absorption of near-infrared photons ($E < E_g$). Several approaches have been developed to tackle these losses and to optimize the conversion of the solar spectrum by solar cells,[3] with the multijunction architecture for example.[4]

An original strategy that has emerged in the last decade to boost the efficiency of the single-junction solar cells is to construct a hybrid device combining photovoltaic conversion with thermoelectric generation. Though several reported experimental photovoltaic-thermoelectric (PV-TE) devices demonstrated they indeed produce more power than a single solar cell,[5–7] the main factor limiting the global efficiency of such PV-TE devices is still the low conversion efficiency of the thermoelectric generator (TEG) (below 8% at ambient temperature).[8] To overcome this limit, one key aspect needs to be considered and has been largely overlooked until recently, namely the interface between the solar cell and the TEG.[5,9–12] Optimizing this interface is crucial in order to fulfill the PV-TE device two pri-

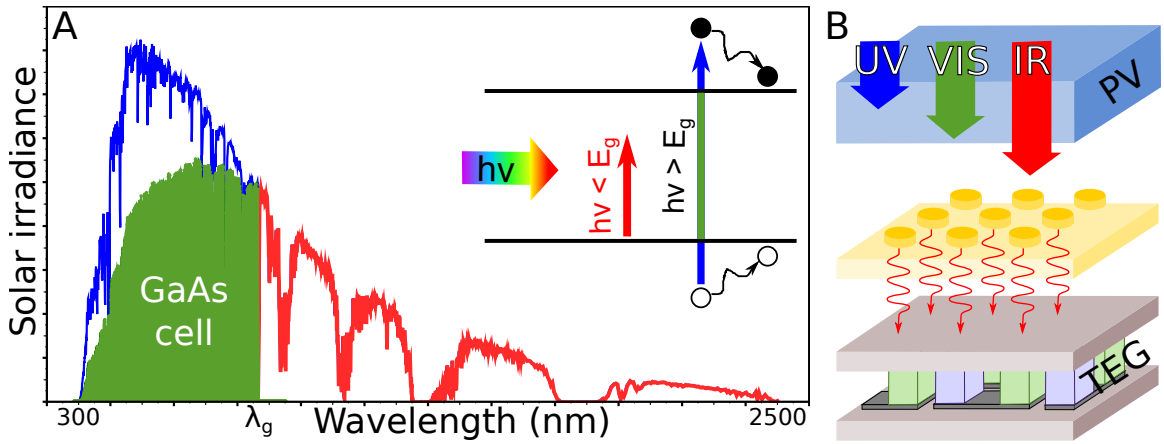

Figure 1: Principle of a hybrid PV-TE device including a photothermal interface. (A) Spectrum of the AM1.5G solar irradiance at the earth's surface showing the energy converted by a GaAs solar cell with $E_g = 1.42$ eV (green) and the intrinsic losses in the cell (thermalization, blue; lack of absorption, red) with the corresponding loss processes schematized in the inset. (B) Schematics of a hybrid photovoltaic-thermoelectric device, including a photothermal interface to convert solar infrared radiation into heat.

mary goals, i.e. to recover the waste heat from the solar cell and to convert the energy of the near-infrared and infrared photons that are not absorbed in the solar cell. Park et al. have shown recently that using a highly conductive thermal material such as boron nitride at the PV-TE interface enables an efficient heat dissipation towards the TEG and, as a consequence, cooling down the solar cell (-7.7°C under 1 sun).[10] Furthermore, integrating a photothermal conversion layer to harvest the solar infrared radiation and converting it into heat allows to heat up the hot contact of the TEG and thus to boost its power output.[9,10] Up till now, only a handful of works have investigated the use of a photothermal interface in PV-TE devices and, to the best of our knowledge, none of them reported the specific spectral design of a photothermal interface to match the solar infrared spectrum for optimal light harvesting.

In this work, we propose a photothermal conversion layer with plasmonic nanoantennas aimed at harvesting solar infrared radiation in hybrid PV-TE devices. Our approach focuses on nanoantennas, that are designed and fabricated to achieve spectrally selective optical and thermal properties, thereby offering the possibility for fine tuning subject to the photovoltaic

material at play. Plasmonic structures have been extensively used in the past to create highly efficient and spectrally selective absorbers, in particular in the infrared range,[13–15] as they provide intense resonant optical properties at tunable frequencies. Photon absorption in metallic nanostructures can subsequently result in heat generation through non-radiative relaxation of hot carriers. Plasmonic nanostructured surfaces have thus been widely studied for photothermal conversion of solar radiation, with various applications,[16,17] including direct solar-heat conversion in TEG devices.[18,19] These metasurfaces are in general tailored to achieve perfect absorption in the visible spectral range (where the solar irradiance is the highest), often at the cost of a limited infrared absorption.

Our original approach consists in the design of plasmonic nanoantennas for the specific photothermal conversion of the solar infrared radiation transmitted through a photovoltaic cell. The challenge is to design and fabricate simple nanostructures that exhibit optimal matching with the solar infrared spectrum (Figure 1A), particularly in the spectral range above the bandgap wavelength of the solar cell of interest (λ_g), i.e. λ_g-2.5 μm. Our study thus used such spectral matching as a key figure of merit. Further, we chose the GaAs solar cell (E_g=1.42 eV, λ_g=0.875 μm), for its high PV conversion efficiency and low sensitivity to temperature. To validate our approach, cm-sized surfaces with nanoantennas are fabricated and thermally characterized.

As a first step, we modeled with discrete dipole approximation (DDA)[20] a single nanoantenna by a cubic mesh of interacting dipoles (see examples in Figure 2A-E). The shape, size and composition of the model nanoantennas are taken into account to calculate the absorption σ_{abs} and scattering σ_{scat} cross-sections in air, under two orthogonal linear polarizations (for complex refractive indices, see Figure S1, Supporting Information).

This is followed by the performances estimates with two main figures of merit. First, the power absorbed by a single nanoantenna under solar infrared illumination, noted P_{abs}, is calculated by weighing σ_{abs} by the AM1.5G solar spectral irradiance (ϕ) and by integrating over the range 0.875-2.5 μm:

$$P_{abs} = \int_{0.875\ \mu m}^{2.5\ \mu m} \sigma_{abs}(\lambda)\phi(\lambda)d\lambda \quad (1)$$

Note that we assume a perfect transmission through the solar cell over the range 0.875-2.5 μm. However, this absorbed power is not always relevant for the performance of the photothermal interface. When designing an absorbing interface, the main factor to consider is the absorption per unit surface. For example, an array of small nanoparticles with low σ_{abs} could in fact harvest more power than one larger particle for the same absorbing surface. So, we define the absorbed power per unit surface P_{abs}^{S} as the absorbed solar power normalized by the area of the particle's base S_{NP}:

$$P_{abs}^{S} = \frac{P_{abs}}{S_{NP}} \quad (2)$$

A key parameter for the design of a photothermal interface, naturally, is the nanoantenna material. We have investigated the impact of the nanoantenna composition on P_{abs} for different geometries (Figure S2, Supporting Information) and have chosen Ni as the best available, having in mind the value of the absorbed power and fabrication constraints, and also the potential material abundance.

Identifying the optimal nanoantenna geometry for a given application is a challenging task with a plethora of nanostructures from spheres and wires to complex star-like geometries reported so far.[21,22] Assessing the fitness for the solar infrared absorption, we scanned through rather simple geometries: nanopads, nanodisks, nanorods and truncated nanocones (Figures 2A-D). We also investigated the diabolo geometry (Figure 2E), its elongated shape and sharp angles being beneficial for high absorption in the near infrared region and its more complex structure offering additional degrees of freedom. For all these investigated structures, the lateral sizes varied between 50 nm and 600 nm, while the height was kept constant at 150 nm taking into account potential nanofabrication constraints. Indeed, for given lateral dimensions, the height of the fabricated structures is limited by the lift-off process.

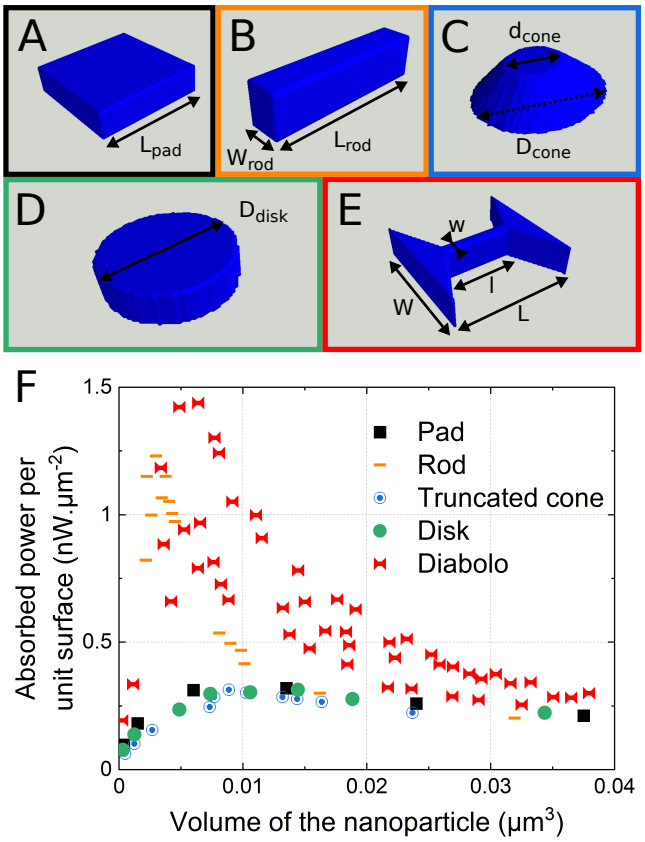

Figure 2: DDA-based numerical simulations of the optical absorption of various nanoantennas. (A-E) 3D representation of the models used for the DDA calculations: (A) pad, (B) rod, (C) cone, (D) disk and (E) diabolo geometries, their varying parameters marked. (F) Absorbed solar power per unit surface P^S_{abs} calculated for 150 nm-thin isolated Ni nanoantennas with different shapes and dimensions.

Table 1: Optical performances of the best isolated Ni nanoantenna for each studied geometry, calculated by DDA numerical simulations. The geometrical parameters are defined in Figures 2A-E.

Geometry and dimensions	Absorbed solar power per antenna (pW)	Absorbed solar power per unit area ($nW/\mu m^2$)	Absorption/scattering power ratio
Diabolo (L=400 nm; W=300 nm; l=300 nm; w=50 nm)	46	1.42	1.81
Rod (L_{rod}=400 nm; W_{rod}= 50 nm)	25	1.23	1.03
Pad (L_{pad}=300 nm)	29	0.32	0.35
Truncated cone (D_{cone}=400 nm; d_{cone}=100 nm)	39	0.31	0.67
Disk (D_{disk}=350 nm)	30	0.31	0.48

Figure 2F displays the calculated P^S_{abs} from Equation 2 for Ni nanoantennas with the different geometries and dimensions, with the best performing summarized in Table 1. Clearly, particles with a volume below 0.01 µm^3 have a better absorption per unit area due to, firstly, blue-shifting the plasmon resonance with a size reduction, and eventually better overlaping

with the solar spectrum; and secondly, by increasing the absorption-over-scattering ratio with decreasing size.[23] However, volumes below 0.005 μm^3 give poorer absorption efficiency.

The optical performances of nanoantennas are strongly influenced by their morphology (Figure 2F). On one hand, nanodisks, nanopads and nanocones exhibit a very similar behavior: P_{abs}^S is not affected by their dimensions for volumes above 0.005 μm^3. On the other hand, P_{abs}^S shows a strong dependence on the dimensions of rod-like nanoantennas, reaching a maximum value of 1.23 nW.μm^{-2} for the antenna with L_{rod}=400 nm and W_{rod}= 50 nm. An even higher P_{abs}^S is achieved with the diabolo shape, outperforming all other geometries (Table 1).

The model nanoantennas evaluated so far (Figure 2) have perfectly smooth surfaces and sharp corners. However, it is well established that nanofabrication introduces surface roughness and often a divergence from the nominal shape and dimensions. We choose to focus on the diabolo nanoantenna (L=540 nm, W=540 nm, l=300 nm and w=50 nm, Figure 3C) to evaluate how these nanodefects affect the optical properties of a nanostructure. Figures 3A-B show electron-beam lithography-fabricated 2D arrays of diabolo nanoantennas (period of 900 nm), where one directly notices, from the SEM and AFM measurements, the deviation of nanoantennas sizes (L=570 nm, W=490 nm, l=270 nm, w=80 nm, Figure 3A) and roughness (Figure 3B) from the nominal design. We thus create two 3D models, taking into account either the deviation in size only (Figure 3D), or both the deviation in size and surface roughness (Figure 3E), and quantify with DDA their absorption of the solar infrared radiation (Figure 3F). The absorption spectrum of the Ni diabolo with the measured dimensions is shifted to longer wavelengths compared to the nominal structure. As a result, the absorption power drops from 75 pW to 66 pW, highlighting the need of control of the lateral dimensions to reach the optimal absorption. Surface roughness, by contrast, has a moderate impact on the absorption spectrum of the particle, similar to what was evidenced in previous works.[24,25] In our case, adding surface roughness induces a slight increase of the absorbed power (67 pW).

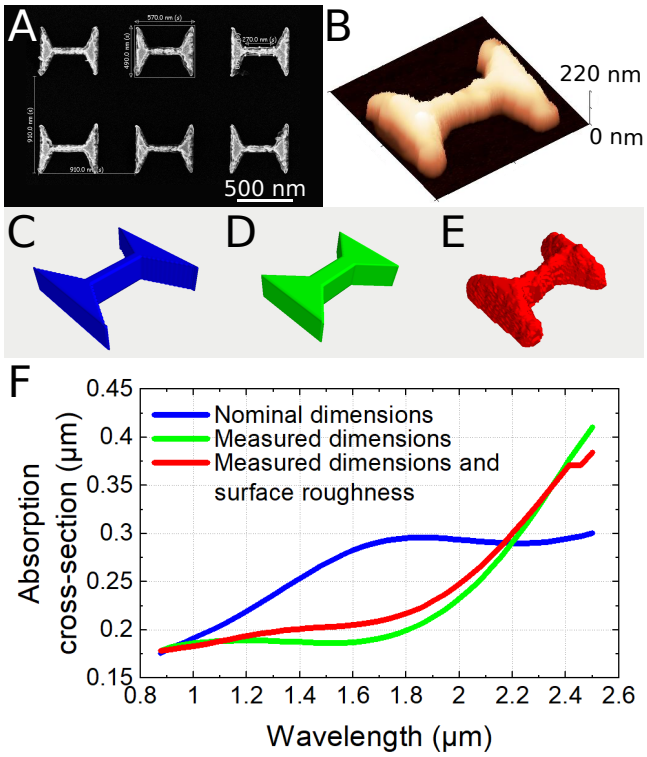

Figure 3: Impact of fabrication defects on the optical properties of Ni diabolo nanoantennas. (A) SEM and (B) AFM images of diabolo-shaped Ni nanoantennas on Si substrate. 3D views of (C) the smooth diabolo with nominal dimensions, (D) the smooth diabolo with measured dimensions and (E) a realistic diabolo with measured dimensions and surface roughness. (F) Calculated absorption spectra of the three structures.

While diabolo nanoantennas have superior absorption power, we further test the temperature evolution upon solar infrared illumination on much simpler nanoantennas (truncated nanocones) with yet reasonable optical performance (Table 1), that can be fabricated into several cm^2 arrays.[26–28] In this way, we are able to measure the temperature resulting from the collective heating effect of a macroscopic array of interacting particles. We thus produced short-range-ordered arrays of truncated nanocone antennas (base diameter of 200 nm) of various metals on top of a glass/silver/alumina substrate (Figures 4A-B). The 100 nm-thick silver layer is used as a mirror reflecting radiations towards the nanoantennas, while the 80 nm-thick alumina layer acts as a dielectric spacer, thus creating a metal-dielectric-metal photonic stack. Using an infrared camera, we measure the temperature of the back side of the substrates (glass) under illumination from the front (antennas).

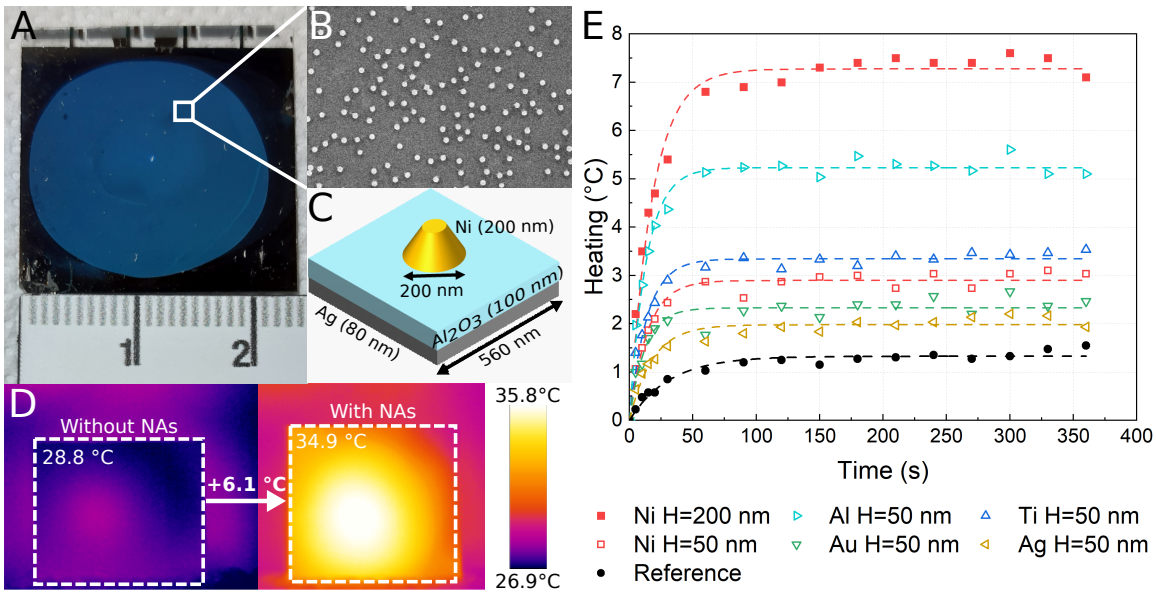

Figure 4: Large-scale photothermal interface. (A) Photograph of one of the fabricated cm^2-sized photothermal interfaces. (B) SEM image of the top surface of a photothermal interface showing a quasi-disordered array of Ni truncated nanocones. (C) Schematics of a nanocone antenna on Ag/alumina. (D) Infrared images of the back sides of the photothermal interface with 200 nm-high Ni nanoantennas and the reference sample (no antennas), when illuminated from the front side. The region across which the temperature is averaged is depicted by the dashed line. (E) Temperature increase of the nanocone antennas surface under AM1.5G, 800-1500 nm, 254 W/m^2 illumination for various nanoantenna materials (dashed lines are guides for an eye).

Illuminating surfaces covered with 50 nm-high cones with a simulated AM1.5G solar spectrum, but limited to the 800-1500 nm range (Figure S4, Supporting Information), we earn temperature increase from 2°C (for Ag) to 5°C (for Al). Furthermore, we demonstrate a 7°C temperature increase when illuminating a sample covered with 200 nm-high Ni truncated nanocones (Figure 4C), which represents a noticeable temperature rise of 6.1°C compared to the reference substrate without nanoantennas (Figure 4D). We believe that even higher temperature could be achieved with 200 nm-high Al particles. For comparison, Park et al. earlier demonstrated 5.1°C temperature increase with a broadband thermal interface material (BN-rGO) integrated in a complete PV-TE device.[10] Kim et al. used a 5 µm thick acrylic film with low thermal conductivity that reached a temperature increase of 30°C under illumination with the full solar spectrum.[9]

Taking into account the surface density of particles, we calculated the temperature increase per particle (see Supporting Information for details). Our 50 nm-high nanocone antennas deliver from 0.5 nK (Ag) to 3.8 nK (Al) increase, while 200 nm-high Ni nanocones only show a 3.3 nK temperature raise. The superior macroscopic temperature achieved by the 200 nm-high Ni nanoantennas is then attributed to a reasonably efficient heating of each single nanoantenna combined with their high density on the surface.

In conclusion, we demonstrate a library of plasmonic nanoantennas for photothermal conversion of solar infrared radiation. We identify diabolo nanoantennas as the most promising, leading to the highest efficiency of infrared solar light harvesting. We highlight the importance of taking into account the fabrication constraints in the design of the practical nanoantennas. We further experimentally demonstrate a 6.1°C temperature rise (compared to a reference substrate) under solar infrared illumination with a cm^2-sized surface of Ni nanocone antennas. This demonstrates the viability of our plasmonic nanoantenna strategy for the infrared radiation conversion by a photothermal interface. We intend to achieve larger temperature increases with denser antenna arrays of diabolo-shaped nanoantennas made using large-area replication techniques such as nanoimprint lithography. We foresee such interface to be straightforwardly integrated in a complete photovoltaic-thermoelectric device, eventually leading to self-sufficient microsystems that use hybrid conversion of solar energy into electricity for power supply. The advantage of our nanoantenna-based approach, as compared to the thin film interface previously used in PV-TE,[9,10] is the decoupling of heat generation and thermal diffusion properties. Indeed, the heat sources are the nanoantennas, which have a small height that renders their thermal resistance negligible, while the thermal distribution in the hybrid system can be regulated by selecting the thermal conductivity of the substrate and encapsulant. Moreover, the use of nanolithography techniques offers control over the position of the particles, which could in the future be leveraged to design systems in which the heat sources are located directly on top of the thermoelectric elements, precisely where the temperature needs to be maximized. Alternatively, our photothermal

interface could prove useful for applications requiring direct solar-thermal conversion, as is the case for solar nanoantenna radiator-based smart windows.[28] We also believe that our design (nanoantenna material, geometrical parameters) could be tuned to match other parts of the solar spectrum, thus being suitable for a broad range of photovoltaic materials.

Acknowledgement

This work was supported by LAAS-CNRS micro and nanotechnologies platform, a member of the Renatech french national network, as well as by the French Agence Nationale de la Recherche under grant ANR-21-CE50-0003 (project HYDRES). The authors also thank the CEMES lab for sharing the IR camera used for thermal characterization. AD and IF acknowledge Swedish Research Council (VR) (Project No. 2017-04828) and Swedish Research Council for Sustainable Development (Formas) (Project No. 2021-01390).

Supporting Information Available

The following files are available free of charge.

- Supporting Information: Additional details on numerical simulations of isolated nanoantennas, fabrication methods and thermal characterization (PDF)

References

(1) Projected Costs of Generating Electricity 2020. `https://www.iea.org/reports/projected-costs-of-generating-electricity-2020`, Date of access: 6th of January 2023.

(2) Hirst, L. C.; Ekins-Daukes, N. J. Fundamental losses in solar cells. *Progress in Photovoltaics: Research and Applications* **2011**, *19*, 286–293.

(3) Green, M. A.; Bremner, S. P. Energy conversion approaches and materials for high-efficiency photovoltaics. *Nature Materials* **2016**, *16*, 23–34.

(4) Geisz, J. F.; France, R. M.; Schulte, K. L.; Steiner, M. A.; Norman, A. G.; Guthrey, H. L.; Young, M. R.; Song, T.; Moriarty, T. Six-junction III–V solar cells with 47.1% conversion efficiency under 143 Suns concentration. *Nature Energy* **2020**, *5*, 326–335.

(5) Wang, N.; Han, L.; He, H.; Park, N.-H.; Koumoto, K. A novel high-performance photovoltaic–thermoelectric hybrid device. *Energy & Environmental Science* **2011**, *4*, 3676.

(6) Park, K.-T.; Shin, S.-M.; Tazebay, A. S.; Um, H.-D.; Jung, J.-Y.; Jee, S.-W.; Oh, M.-W.; Park, S.-D.; Yoo, B.; Yu, C.; Lee, J.-H. Lossless hybridization between photovoltaic and thermoelectric devices. *Scientific Reports* **2013**, *3*, 2123.

(7) Lorenzi, B.; Mariani, P.; Reale, A.; Di Carlo, A.; Chen, G.; Narducci, D. Practical development of efficient thermoelectric – Photovoltaic hybrid systems based on wide-gap solar cells. *Applied Energy* **2021**, *300*, 117343.

(8) KELK Ltd. > Product information on thermo modules. `https://www.kelk.co.jp/english/generation/data_1.html#data_1_1`, Date of access: 6th of January 2023.

(9) Kim, Y. J.; Choi, H.; Kim, C. S.; Lee, G.; Kim, S.; Park, J.; Park, S. E.; Cho, B. J. High-Performance Monolithic Photovoltaic–Thermoelectric Hybrid Power Generator Using an Exothermic Reactive Interlayer. *ACS Applied Energy Materials* **2019**, *2*, 2381–2386.

(10) Park, Y.; Cho, K.; Yang, S.; Park, T.; Park, S.; Song, H.-e.; Kim, S. M.; Kim, S. Performance of Hybrid Energy Devices Consisting of Photovoltaic Cells and Thermoelectric Generators. *ACS Applied Materials & Interfaces* **2020**, *12*, 8124–8129.

(11) Zhang, J.; Zhai, H.; Wu, Z.; Wang, Y.; Xie, H. Experimental investigation of novel in-

tegrated photovoltaic-thermoelectric hybrid devices with enhanced performance. *Solar Energy Materials and Solar Cells* **2020**, *215*, 110666.

(12) Park, Y.; Cho, K.; Kim, S. Performance Prediction of Hybrid Energy Harvesting Devices Using Machine Learning. *ACS Applied Materials & Interfaces* **2022**, *14*, 11248–11254.

(13) Brown, L. V.; Yang, X.; Zhao, K.; Zheng, B. Y.; Nordlander, P.; Halas, N. J. Fan-Shaped Gold Nanoantennas above Reflective Substrates for Surface-Enhanced Infrared Absorption (SEIRA). *Nano Letters* **2015**, *15*, 1272–1280.

(14) Mitobe, D.; Suzuki, Y.; Shimada, T. Local enhanced site in surface enhanced infrared absorption with gold nano particle array by Rigorous coupled-wave analysis. *Journal of Physics Communications* **2020**, *4*, 115009.

(15) Bagheri, S.; Zgrabik, C. M.; Gissibl, T.; Tittl, A.; Sterl, F.; Walter, R.; De Zuani, S.; Berrier, A.; Stauden, T.; Richter, G.; Hu, E. L.; Giessen, H. Large-area fabrication of TiN nanoantenna arrays for refractory plasmonics in the mid-infrared by femtosecond direct laser writing and interference lithography [Invited]. *Optical Materials Express* **2015**, *5*, 2625.

(16) Liu, G.; Xu, J.; Chen, T.; Wang, K. Progress in thermoplasmonics for solar energy applications. *Physics Reports* **2022**, *981*, 1–50.

(17) Cheng, P.; Wang, D.; Schaaf, P. A Review on Photothermal Conversion of Solar Energy with Nanomaterials and Nanostructures: From Fundamentals to Applications. *Advanced Sustainable Systems* **2022**, *6*, 2200115.

(18) Pan, Y.; Tagliabue, G.; Eghlidi, H.; Höller, C.; Dröscher, S.; Hong, G.; Poulikakos, D. A Rapid Response Thin-Film Plasmonic-Thermoelectric Light Detector. *Scientific Reports* **2016**, *6*, 37564.

(19) Kosuga, A.; Yamamoto, Y.; Miyai, M.; Matsuzawa, M.; Nishimura, Y.; Hidaka, S.; Yamamoto, K.; Tanaka, S.; Yamamoto, Y.; Tokonami, S.; Iida, T. A high performance photothermal film with spherical shell-type metallic nanocomposites for solar thermoelectric conversion. *Nanoscale* **2015**, *7*, 7580–7584.

(20) Draine, B. T.; Flatau, P. J. Discrete-Dipole Approximation For Scattering Calculations. *Journal of the Optical Society of America A* **1994**, *11*, 1491.

(21) Kretschmer, F.; Mühlig, S.; Hoeppener, S.; Winter, A.; Hager, M. D.; Rockstuhl, C.; Pertsch, T.; Schubert, U. S. Survey of Plasmonic Nanoparticles: From Synthesis to Application. *Particle & Particle Systems Characterization* **2014**, *31*, 721–744.

(22) Lu, X.; Rycenga, M.; Skrabalak, S. E.; Wiley, B.; Xia, Y. Chemical Synthesis of Novel Plasmonic Nanoparticles. *Annual Review of Physical Chemistry* **2009**, *60*, 167–192.

(23) Young, A. T. Rayleigh scattering. *Applied Optics* **1981**, *20*, 533–535.

(24) Trügler, A.; Tinguely, J.-C.; Krenn, J.; Hohenau, A.; Hohenester, U. Influence of surface roughness on the optical properties of plasmonic nanoparticles. *Physical Review B* **2011**, *83*, 081412(R).

(25) Kildishev, A. V.; Borneman, J. D.; Chen, K.-P.; Drachev, V. P. Numerical Modeling of Plasmonic Nanoantennas with Realistic 3D Roughness and Distortion. *Sensors* **2011**, *11*, 7178–7187.

(26) Fredriksson, H.; Alaverdyan, Y.; Dmitriev, A.; Langhammer, C.; Sutherland, D. S.; Zäch, M.; Kasemo, B. Hole–Mask Colloidal Lithography. *Advanced Materials* **2007**, *19*, 4297–4302.

(27) Jonsson, G. E.; Miljkovic, V.; Dmitriev, A. Nanoplasmon-enabled macroscopic thermal management. *Scientific Reports* **2014**, *4*, 5111.

(28) Jönsson, G.; Tordera, D.; Pakizeh, T.; Jaysankar, M.; Miljkovic, V.; Tong, L.; Jonsson, M. P.; Dmitriev, A. Solar Transparent Radiators by Optical Nanoantennas. *Nano Letters* **2017**, *17*, 6766–6772.